ACS OMEGA

http://pubs.acs.org/journal/acsodf

Article

Polyethyleneimine-Starch Functionalization of Single-Walled Carbon Nanotubes for Carbon Dioxide Sensing at Room Temperature

Samrah Manzoor, Mohammad Talib, Aleksey V. Arsenin, Valentyn S. Volkov, and Prabhash Mishra*

Cite This: *ACS Omega* 2023, 8, 893−906

Read Online

ACCESS | Metrics & More | Article Recommendations | Supporting Information

ABSTRACT: There is an ever-growing interest in the detection of carbon dioxide (CO_2) due to health risks associated with CO_2 emissions. Hence, there is a need for low-power and low-cost CO_2 sensors for efficient monitoring and sensing of CO_2 analyte molecules in the environment. This study reports on the synthesis of single-walled carbon nanotubes (SWCNTs) that are functionalized using polyethyleneimine and starch (PEI-starch) in order to fabricate a PEI-starch functionalized SWCNT sensor for reversible CO_2 detection under ambient room conditions (T = 25 °C; RH = 53%). Field-emission scanning electron microscopy, high-resolution transmission electron microscopy, Raman spectroscopy, and Fourier transform infrared spectroscopy are used to analyze the physiochemical properties of the as-synthesized gas sensor. Due to the large specific surface area of SWCNTs and the efficient CO_2 capturing capabilities of the amine-rich PEI layer, the sensor possesses a high CO_2 adsorption capacity. When exposed to varying CO_2 concentrations between 50 and 500 ppm, the sensor response exhibits a linear relationship with an increase in analyte concentration, allowing it to operate reliably throughout a broad range of CO_2 concentrations. The sensing mechanism of the PEI-starch-functionalized SWCNT sensor is based on the reversible acid−base equilibrium chemical reactions between amino groups of PEI and adsorbed CO_2 molecules, which produce carbamates and bicarbonates. Due to the presence of hygroscopic starch that attracts more water molecules to the surface of SWCNTs, the adsorption capacity of CO_2 gas molecules is enhanced. After multiple cycles of analyte exposure, the sensor recovers to its initial resistance level via a UV-assisted recovery approach. In addition, the sensor exhibits great stability and reliability in multiple analyte gas exposures as well as excellent selectivity to carbon dioxide over other interfering gases such as carbon monoxide, oxygen, and ammonia, thereby showing the potential to monitor CO_2 levels in various infrastructure.

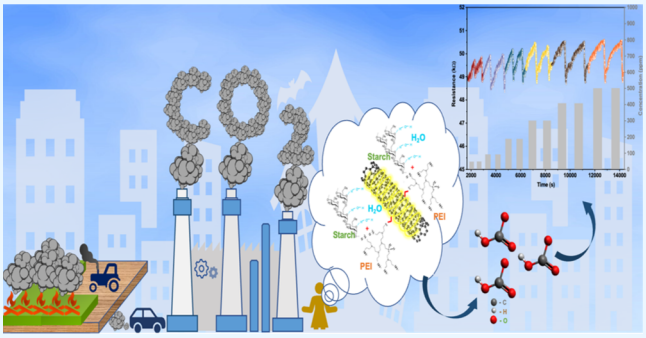

1. INTRODUCTION

Greenhouse gas emissions have reached new heights in recent years as a result of increased industrialization, biochemical activities, and vehicular emissions. As a result, there has been an increase in pollution levels, harmful chemical species, and toxins as well as the warming of the planet caused by the abundance of heat-trapping greenhouse gases in the atmosphere.[1,2] Continuous exposure to highly toxic gases can lead to lethal respiratory disorders such as asthma and chronic obstructive pulmonary disease.[3] In particular, carbon dioxide (CO_2) is regarded as the primary anthropogenic contributor to climatic change and global warming, thereby drawing the attention of researchers globally.[4−6] As per the latest Greenhouse Gas Bulletin published by the World Meteorological Organization (WMO), the amount of CO_2 in the atmosphere has crossed the 400 ppm mark in 2015, and just within a span of 5 years it has reached 413.2 ppm in 2020. This accounts for about 149% increase in comparison with pre-industrial times, when humans started disturbing Earth's natural ecosystem. The Bulletin reports that the warming effect on our climate by greenhouse gases escalated by 47% from 1990 to 2020, with carbon dioxide being responsible for about 80% of this increase.[7] Moreover, prolonged exposure in closed environments such as space capsules and submarines might result in dizziness or headache, which can lead to health issues such as breathing difficulty and oblivion, making CO_2 detection at low concentrations a critical technology.[8] In this regard, significant efforts have been made in recent years to develop practical and extremely sensitive gas sensors capable of detecting CO_2 at low concentrations.[9−11]

Received: September 27, 2022
Accepted: December 5, 2022
Published: December 20, 2022

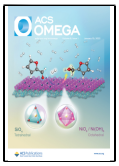

As of now, diverse CO_2 gas sensing protocols have been utilized, including gas−liquid chromatography,[12] mass spectrometry,[13] non-dispersive infrared (NDIR) gas analyzer,[14] and optical-,[15,16] electrochemical-,[17−19] surface and bulk acoustic wave (SAW and BAW)-,[20] work function-,[21,22] capacitive-,[23] and chemiresistive-based[5] sensing. However, in comparison with chemiresistive sensing devices, other devices suffer from many disadvantages, such as high maintenance costs (gas−liquid chromatography, mass spectrometry), influence of interfering gaseous species (acoustic wave- and work function-based), expensive fabrication processes and miniaturization (optical), short device life (electrochemical), high energy consumption (NDIR), and difficulty in capacitance measurements (capacitive), thus restricting their usage. Chemiresistive sensors have generated high demand due to their good sensitivity, small size, minimal power consumption, low cost, longer stability, and room-temperature operation.[5,24] In this approach, diverse organic as well as inorganic sensing materials have been investigated to develop CO_2 sensors. Metal oxide semiconductors (MOS) have been widely explored for use in gas sensors owing to their low cost, ease of operation, high reliability, and sensitivity.[2] Xiong et al.[25] reported that owing to the porous nanofibers of 8 at % La−SnO_2 structures, this sensor demonstrated maximum response (∼3.7) toward 1000 ppm CO_2 analyte with response/recovery times of 24 s/92 s at an operating temperature of 300 °C. Kanaparthi et al.[26] reported the use of ZnO nanoflakes to develop a highly sensitive (0.1125 for 600 ppm CO_2), ultrafast (response/recovery times in the sub-20 s range), and reversible CO_2 gas sensor working in the concentration range of 400−1025 ppm. However, MOS-based gas sensors suffer from short device life and high power consumption due to the requirement of high operating temperatures.[26] On the other hand, carbon-based nanomaterials, such as carbon nanotubes, graphene, and reduced graphene oxide, have attracted researchers' attention due to their unique properties, such as high surface area-to-volume ratio, excellent carrier mobility, room temperature (RT) operation, hydrophobic nature, and longer stability at RT.[28−30] Furthermore, 2D materials such as MoS_2,[31] SnS_2,[32] and others have been investigated for gas sensing applications due to their large specific area, tunable band gap, high carrier mobility, and variety of active sites. These materials have been combined with other materials such as MOS[33] and MXenes[34] to form heterostructures, which improves gas adsorption properties. Smith et al.[28] presented graphene-based CO_2 sensing and analyzed its cross-sensitivity with humidity. Although they observed virtually no responses from N_2, Ar, and O_2, there appeared to be a significant cross-sensitivity between carbon dioxide and humidity at high CO_2 concentrations. Zhang et al.[29] recently reported the synthesis of random and horizontally aligned CNTs modified by covalent functionalization using diazonium tetrafluoroborate (4-BBDT). It was observed that horizontally aligned CNTs provided shorter response/recovery times of 33 s/46 s because of the absence of inter-tube CNT junctions, while random CNTs provided a larger sensor response owing to the overlap of electronic states in randomly oriented CNT walls, which might have led to the availability of a greater number of conduction channels. Li et al.[30] reported the synthesis of nitrogen-doped reduced graphene oxide (N-rGO) and ZnO-based nitrogen-doped reduced graphene oxide (N-rGO-ZnO) porous nanomaterials and showed that the CO_2 and N_2 adsorption capability of N-rGO-ZnO is larger than that of N-rGO at lower temperatures.

Since CO_2 is a relatively stable and unreactive molecule, developing a highly sensitive CO_2 gas sensor poses some challenges. Single-walled carbon nanotubes (SWCNTs) are attractive candidates in sensing applications, being responsive toward both charge acceptors and donors but not against weak Lewis acids or bases such as CO_2.[29] Sensing response to CO_2 can be enhanced by using a detection layer that stimulates a chemical reaction with the analyte molecules, thus altering the properties of the SWCNT sensor. In this approach, functionalization of SWCNTs by employing polymer coating presents the advantage of less degree of distortion of the electronic and physical properties of nanotubes.[35−38] Based on the HSAB (Hard Soft Acid Base) theory, researchers have developed various novel CO_2 recognition layers, such as polyethyleneimine (PEI),[39] polyamide (PA),[35] diethanolamine (DEA),[40] and so on, which are hard bases and can effectively capture the CO_2 gas. Han et al.[39] developed a PEI-functionalized CNT thin-film room-temperature sensor using a filtration method and proposed that owing to the reversible acid−base equilibrium interaction between the amine moieties of PEI and CO_2 molecules, the functionalized CNT sensor exhibited better sensing responses than the pristine CNT sensor. Zainab et al.[35] reported the development of a free-standing polyamide/CNT membrane with PEI impregnation that could successfully capture an optimum of ∼51 mg CO_2 for each gram of the fabricated membrane, with consistent performance up to 12 successive cycles of adsorption/desorption, proving high device stability. Thus, a base-type amino group-containing polymer wrapped around CNTs could be an efficient method for detecting acidic gases like CO_2 at room temperature.However, under dry conditions, the adsorption capacity is limited due to less protonation of amino groups of the polymer (such as PEI). Therefore, a hygroscopic polymer such as starch or polyethylene glycol must be incorporated into the PEI-functionalized CNTs in order to attract more water molecules to the CNT surface and thus shift the equilibrium due to the competing formation of carbonates and bicarbonates.[41−43] The collaborative effect can be achieved by incorporating the characteristics of SWCNTs, PEI, and starch in the fabrication of the CO_2 gas sensor. In this regard, SWCNTs are excellent candidates for gas sensing materials due to their large specific surface area and abundant binding sites for gas adsorption, high responsivity at low temperatures, high carrier mobility, as well as their hollow structure, high aspect ratio, and biocompatibility.[39] In addition, chemical functionalization of SWCNTs with selectors or receptors can result in sensors that are selective to specific analytes. The amine-rich polymer PEI has large CO_2 adsorption capabilities due to the reversible acid−base chemical reactions between the amine groups (primary, secondary, and tertiary) of PEI and CO_2 molecules. Starch, being hygroscopic in nature, provides more water molecules for acid−base reactions. Water vapor plays a critical role in the adsorption of CO_2 gas molecules. While it restricts the CO_2 adsorption capability of hydrophilic materials such as MXenes,[44,45] it enhances the adsorption capacity of hydrophobic materials, such as CNTs. Therefore, the objective of this work is to develop a chemiresistive sensor by integrating the potential benefits of SWCNTs, PEI, and starch, which can be primarily utilized for CO_2 detection in a concentration

https://doi.org/10.1021/acsomega.2c06243
ACS Omega 2023, 8, 893−906

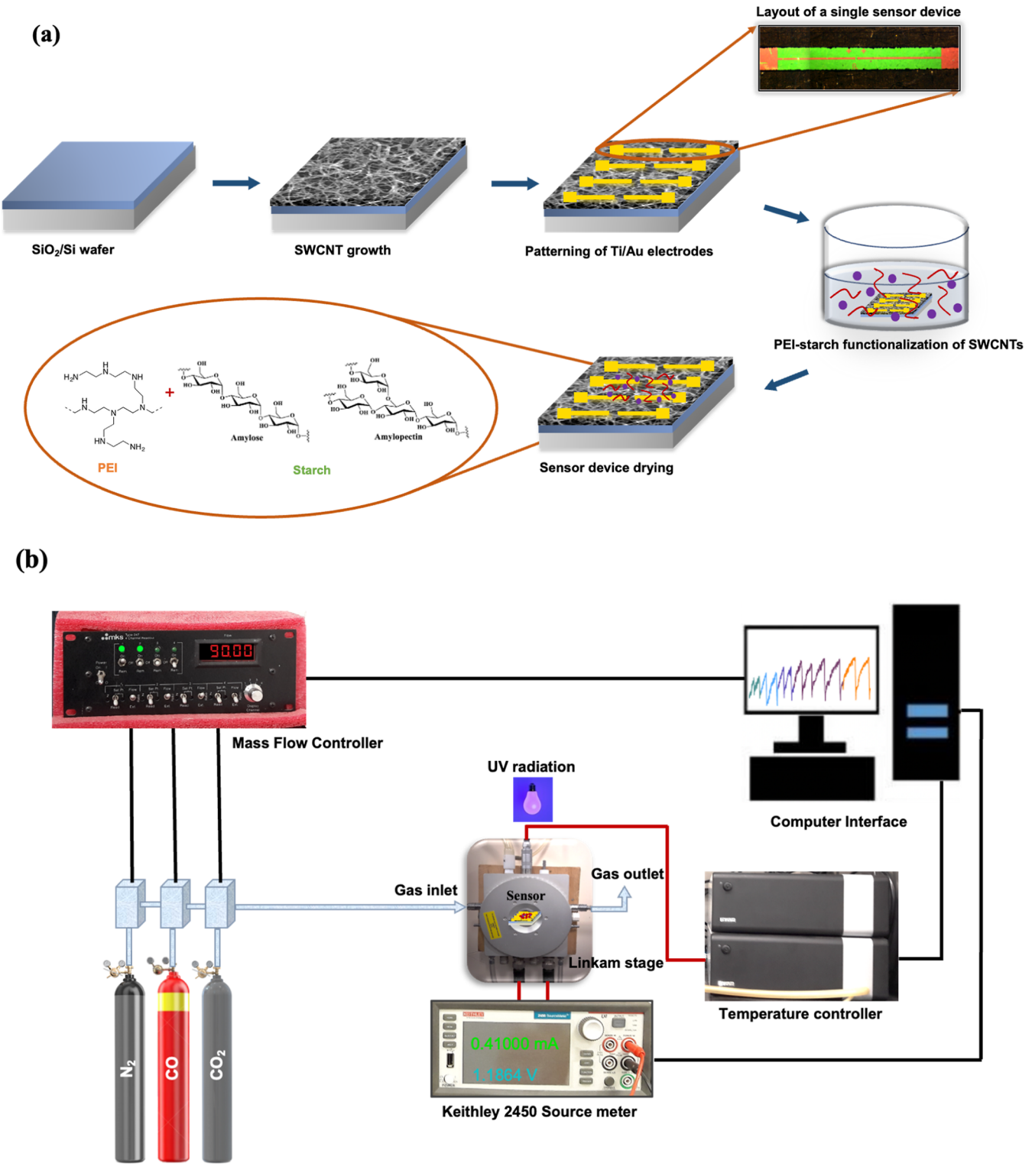

Figure 1. (a) Schematic diagram for the fabrication of a PEI-starch-functionalized SWCNTs gas sensor device; (b) Experimental setup for sensor testing.

range of 50−500 ppm while working under ambient room conditions.

Herein, we synthesized random SWCNT networks via a conventional thermal-chemical vapor deposition technique on a SiO_2/Si substrate. The electrodes were patterned using conventional photolithography and lift-off processes. For efficient CO_2 detection, PEI-starch was incorporated for functionalization of the SWCNTs. The as-fabricated sensor exhibited good sensor response, a competitive response time for room-temperature sensors, and ultrafast and stable recovery by means of UV irradiation. The sensor also displayed excellent cross-sensitivity with other interfering gases such as carbon monoxide, ammonia, and oxygen. The sensor demonstrated good reliability and repeatability, implying that

https://doi.org/10.1021/acsomega.2c06243
ACS Omega 2023, 8, 893−906

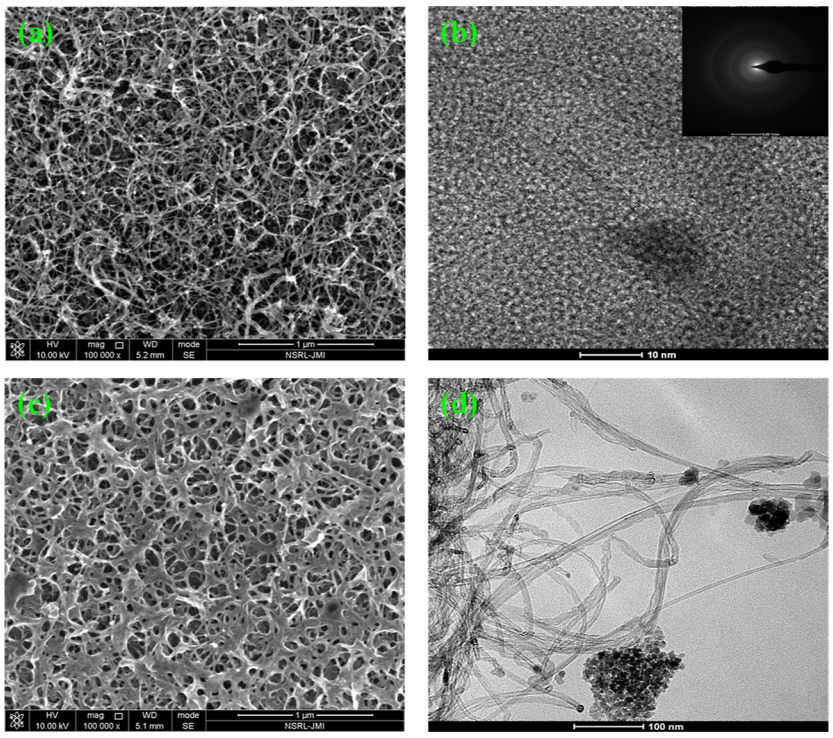

Figure 2. (a–b) SEM and TEM micrographs of the as-grown pristine SWCNTs, respectively (inset show the SAED pattern); (c–d) SEM and TEM micrographs for the PEI-starch-sfunctionalized SWCNTs.

it could be an efficient gas sensor with the potential to be utilized for monitoring the environmental limit of CO_2.

2. EXPERIMENTAL SECTION

2.1. Materials. SWCNT random networks were grown by a conventional thermal-chemical vapor deposition technique on a 300 nm thick SiO_2 layer deposited thermally onto the Si substrate. Polyethyleneimine (PEI) with an average $M_w \sim$ 25,000 (Sigma-Aldrich Co., Ltd.) was employed for the functionalization of SWCNT networks. Starch soluble with an average $M_w \sim$ 10,000 (Thermo Fisher Scientific Co., Ltd.) was added for its hygroscopic properties. Deionized (DI) water was utilized from the Millipore DI water purification system. All the reagents involved in this study were of analytical grade and used without further processing.

2.2. Fabrication of a PEI-Starch-Functionalized SWCNT Gas Sensor Device. For preparing a device based on as-grown SWCNT networks, two coplanar Ti/Au (10:100 nm) electrodes were deposited via RF sputtering onto the top layer of SiO_2, followed by conventional photolithography and patterning of electrodes by lift-off processes. The channel length between the two electrodes was ~8 μm; this single-channel device was implemented for further procedures.

After performing fundamental electrical measurements to validate device characteristics, the SWCNTs network film was impregnated with a co-polymer coating to improve the SWCNTs' sensitivity toward CO_2. Therefore, a typical solution was prepared by dissolving 0.5 mL of PEI and 0.25 g of starch in DI water (solvent) and stirring magnetically until the mixture became homogeneous. Subsequently, the device was immersed in a PEI-starch solution for 12 h and rinsed carefully with DI water, then dried in the oven at room temperature before testing. Figure 1a schematically describes the steps employed for the fabrication of a PEI-starch-functionalized SWCNT device for gas sensing applications.

2.3. Analytical Methods. The structural morphology of the as-grown SWCNT random networks and PEI-starch-functionalized SWCNTs was explored by employing a field-emission scanning electron microscope (Nova Nano SEM 450, FEI) at an accelerating voltage of 10 kV. The microstructure, SWCNT interlayer spacing, and selected area electron diffraction (SAED) pattern of the as-grown SWCNTs were observed with a transmission electron microscope (JEOL JEM F-200). The comparison of Raman modes for pristine SWCNT networks and PEI-starch-functionalized SWCNTs was probed by the micro-Raman spectrophotometer (Lab RAM HR800, HORIBA J.Y.) at a laser wavelength of 532 nm. The chemical functionalization of the examined materials was characterized by a Nicolet iS50 FTIR spectrometer (Thermo Scientific). The electrical characterization of the fabricated sensor device was analyzed using a Keithley 2450 Source Meter by SMU Instrument (Tektronix).

2.4. Gas Sensing Measurements. The sensing properties of pristine SWCNT and PEI-starch-functionalized SWCNT devices were tested in a sealed chamber under ambient conditions. As depicted in Figure 1b, the sensor device was fixed on a Linkam stage connected to both the temperature controller and the gas mixing apparatus. The gas sensors' response to carbon dioxide (CO_2), carbon monoxide (CO), oxygen (O_2), and ammonia (NH_3) were distinguished by exposing the devices to varying concentrations of the analyte gas. Certified 500 ppm CO_2, 1000 ppm CO, 5 vol % O_2, and 300 ppm NH_3 cylinders were used in dilution. Research-grade (99.999% purity) N_2 gas was used instead of air as a carrier gas since the addition of synthetic air will induce a mixed response of the analyte gas and oxygen in the carrier gas; hence, it will be difficult to determine the mechanism of interaction between

https://doi.org/10.1021/acsomega.2c06243
ACS Omega 2023, 8, 893–906

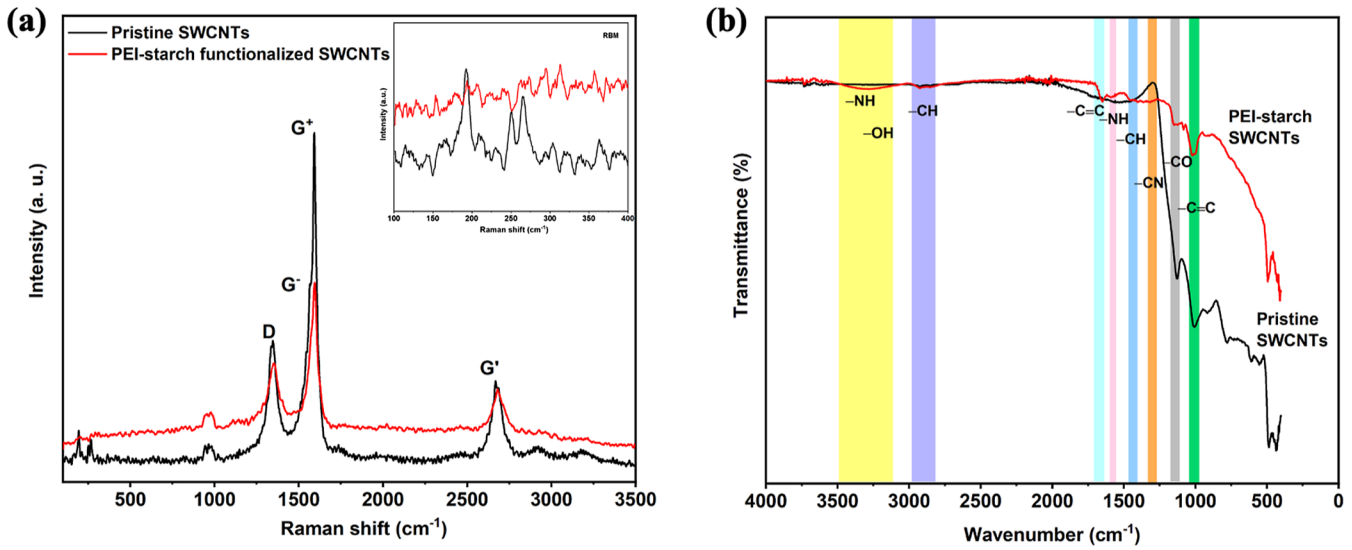

Figure 3. (a) Raman spectra of as-grown pristine SWCNTs, and PEI-starch-functionalized SWCNTs (the inset shows the comparison of RBMs before and after functionalization); (b) FTIR spectra of as-grown pristine SWCNTs, and PEI-starch-functionalized SWCNTs.

target gases and functionalized SWCNTs.[46] To minimize the risk of experimental aberrations, the concentration of analyte gases was modified by carrying out a systematic mixing of carrier and analyte gases controlled by two mass flow controllers (MFCs) from MKS Instruments with a full scale of 500 sccm and 100 sccm, respectively. The concentration of CO_2 gas was varied from 50 ppm to 500 ppm, with the total flux rate fixed at 100 sccm. The electrical resistances of the sensor devices were measured by a Keithley 2450 Source Meter at a constant bias voltage of 12 V, which was automated with the use of KickStart software 2020. For the fast recovery of the sensor device, UV illumination in the wavelength range of 280−330 nm was fixed over the sensing chamber. The sensor device was allowed to reach a stable baseline value in the presence of N_2 gas under ambient operating conditions of $T = (25 \pm 2)°C$; RH = (50 ± 3) %.

Figure 1b illustrates the schematic for the PEI-starch-functionalized SWCNT-based gas sensor testing setup. The sensor resistance in the presence of N_2 (R_a) and analyte gas (R_g) was recorded, and the sensor response was evaluated using the following equation

$$S(\%) = \frac{|R_g - R_a|}{R_a} \times 100 \quad (1)$$

where S represents the gas sensor response, R_g and R_a denote the final and initial values of resistances on exposure to analyte gas and inert N_2 gas, respectively.

3. RESULTS AND DISCUSSION

3.1. Characterizations of Pristine SWCNTs and PEI-Starch-Functionalized SWCNTs. Field emission scanning electron microscopy (FESEM) and high-resolution transmission electron microscopy (HRTEM) were used to analyze the morphological and microstructure characteristics of the synthesized gas sensors. Figure 2a,b displays SEM and TEM micrographs of the as-grown pristine SWCNTs. The SEM illustration shows randomly oriented single-wall nanotubes that exist in a bundle form due to the Van der Waals interaction between adjacent SWCNTs.[47] The average diameter of these SWCNT bundles is in a range of 7−9 nm (as shown in Figure S1a). The high-resolution TEM image represents the clear lattice fringes of SWCNTs with an interlayer spacing of d_{002} = 0.352 nm, corresponding to the d-spacing of (002) planes, while the inset of Figure 2b displays the selected area diffraction pattern (SAED). The innermost reflection ring (002) is associated with the (002) diffraction of the hexagonal graphite structure in as-grown SWCNTs.[48] Figure 2c shows the SEM micrograph of PEI-starch-functionalized SWCNTs, where it can be seen that SWCNT bundles were wrapped by the polymer. This PEI-starch impregnation enveloped most of the SWCNTs and, as a result, formed a sticking structure between the adjacent SWCNT bundles. Thus, a homogeneous coating of PEI-starch is developed over the SWCNTs network, and the average diameter of these SWCNT bundles increases to about 13−17 nm (as shown in Figure S1b). The TEM micrograph of PEI-starch-functionalized SWCNTs suggests a polymer coating on the SWCNTs' surface, as shown in Figure 2d.

The characteristic vibrational modes of the as-grown pristine SWCNTs and PEI-starch-functionalized SWCNTs were analyzed by using Raman spectroscopy with the incident laser excitation wavelength of 532 nm, maintaining a spot size of 1.19 μm at the sample surface under ambient conditions (Figure 3a). The Raman spectra of pristine SWCNTs exhibit sharp peaks at 1336 cm^{-1}, G^- = 1568 cm^{-1}, and G^+ = 1584 cm^{-1}, denoting the characteristic D and G bands of carbon-based nanomaterials, respectively. The first order tangential G band, analogues to the vibrations of E_{2g} mode, originates due to the vibrational frequency of higher energy of sp2 carbon atoms and gives rise to multi-peak characteristic because of the symmetry disturbance of the tangential vibration due to rolling of a graphene sheet into a cylindrical tube. Whereas, the second-order D band results from the disordered carbons, vacancies, and grain boundaries.[49] The I_D/I_G ratio of the intensities of the G and D bands represents the amount of defects in CNT, as calculated from Figure 3, I_D/I_G = 0.594 for pristine SWCNTs. Another peak in the spectra of most carbon-based nanomaterials is the G′(2D, also known as an overtone of the D band) band, appearing at ∼2670 cm^{-1} for as-grown pristine SWCNTs. This high-frequency peak is associated with Raman scattering due to a vibrational mode defined by the

https://doi.org/10.1021/acsomega.2c06243
ACS Omega 2023, 8, 893−906

breathing of six carbon atoms associated with a hexagon in the hexagonal lattice structure of graphene.[50] One of the important aspects of the graphene-related materials and unique among SWCNTs is the so-called radial breathing mode (RBM), and this vibration has a sharp peak in as-grown SWCNTs at 192 cm^{-1} (Figure 3a). This vibrational mode occurs due to the cylindrical configuration of a nanotube, in which the radius of the nanotube oscillates. The RBM determines the diameter of an SWNT and is given by the following equation[51]

$$\omega_{RBM} = \frac{248}{d_t} \quad (2)$$

where ω_{RBM} is the RBM frequency (in cm^{-1}), and d_t is the nanotube diameter (in nm). From eq 2, the diameters of SWCNTs were measured in a range of 0.93−2.12 nm.

The PEI-starch functionalization results were established by comparing the position and intensity of Raman vibrational modes before and after the functionalization of SWCNTs. As presented in Figure 3a, the graphitic G-band, defect-related *D*-band, and the overtone *G*′(or, 2D) shifted to G^- = 1577 cm^{-1} and G^+ = 1593, 1345, and 2679 cm^{-1}, respectively. This blue-shift phenomenon can be explained by the interaction between the lone pair e^- of amine functional groups ($-NH_2$) in the chains of PEI and π-electrons of SWCNT. Hence, the SWCNT electron-density was enhanced, and the polarization of SWCNTs was increased owing to the p-π conjugation of SWCNTs.[52,53] In addition, the PEI-starch functionalization resulted in the dispersion of radial breathing modes (RBMs), and the spectrum exhibits no sharp peaks for RBMs (inset of Figure 3a). Besides, a decrease in the Raman peak intensities and an increase in the I_D/I_G ratio (0.732) of the PEI-starch-functionalized SWCNTs, in comparison with as-grown pristine SWCNTs affirms the surface wrapping by PEI on SWCNTs, giving rise to some surface modification of SWCNTs.[54] Table 1 compares the raman peaks of the as-grown SWCNTs and PEI-starch functionalized SWCNTs.

Table 1. Comparative Raman Analysis of SWCNTs before and after PEI-Starch Functionalization

material	RBM (cm−1)	G^+ (cm^{-1})	G^- (cm^{-1})	*D* (cm^{-1})	G′ (2D) (cm^{-1})
as-grown SWCNTs	192	1584	1568	1336	2670
PEI-starch-functionalized SWCNTs	dispersed	1593	1577	1345	2679

The FT-IR analysis of both as-grown pristine SWCNTs and PEI-starch-functionalized SWCNTs was implemented to verify the presence of functional groups impregnated on the surfaces of PEI-starch-functionalized SWCNT structures, as shown in Figure 3b. The spectrum of PEI-starch-functionalized SWCNTs possesses some characteristic peaks specific to amine functional groups, such as ∼3320 cm^{-1} (N−H stretching), 2925−2856 cm^{-1} (C−H stretching and O−H stretching), ∼1588 cm^{-1} (N−H bending), ∼1455 cm^{-1} (C−H bending), and ∼1318 cm^{-1} (C−N stretching).[52−59] Few absorption bands prevail in both functionalized and unfunctionalized SWCNTs, which correspond to C═C stretching (∼1650 cm^{-1}), C−O stretching (∼1134 cm^{-1}), and C═C bending (∼1006 cm^{-1}). The distribution of SWCNT diameters for as-grown SWCNTs illustrates broadness in the C═C vibrational band, implying that the broad band is made up of several component bands.[60,61] Therefore, the functionalization results affirm effective grafting of PEI-starch onto the nanotube surfaces.

3.2. Electrical Properties of Fabricated Devices. To analyze the transport behavior of the pristine SWCNTs and PEI-starch-functionalized SWCNT devices, the electrical measurements were carried out by plotting the current−voltage (*I*−*V*) characteristics under ambient room conditions [*T* = (25 ± 2)°C; RH = (50 ± 3) %] in a uniform N_2 gas flow. The *I*−*V* curves were attained by sweeping the applied voltage from −12 to 12 V, as shown in Figure 4a. Since the influence

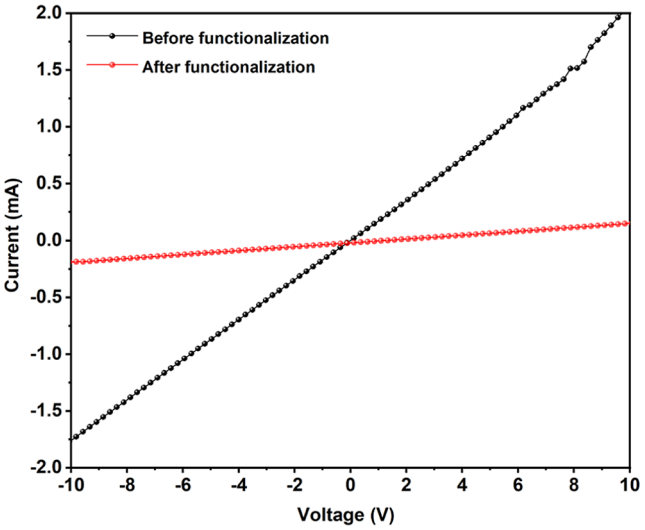

Figure 4. *I*−*V* characteristics for as-grown pristine SWCNTs and PEI-starch-functionalized SWCNTs under ambient room conditions.

of contact resistance between the SWCNTs network and electrodes (Ti/Au) was observed to be negligible, we assume that the electrical transport response is from the SWCNTs network. As illustrated in Figure 4a, the I−V curves possess linear behavior, suggesting the ohmic conduction between the electrodes and SWCNTs. According to Kong *J* et al.,[62] using Ti/Au as a contact material may result in Ohmic contact. This may also be attributed to the phenomenon of quantum tunneling of charge carriers between metal/semiconductor interface.[63] The real-time monitoring of resistance (*R*) versus time (*t*) for pristine as-grown SWCNTs when the operating temperature (*T*) is increased to 100 °C is shown in Figure S2. It clearly shows that resistance gradually falls with time with an increase in temperature until it reaches a steady value, which is an established property of semiconducting behavior.[27]

The *I*−*V* curve of SWCNTs after PEI-starch functionalization (in Figure 4a) shows decreased electrical current and thus increased resistance for charge carrier transport. This may be due to some modifications (or defects) introduced in SWCNTs as a result of functionalization. The defect creation in PEI-starch-functionalized SWCNTs was confirmed by the increase in I_D/I_G ratio in Raman spectra after functionalization. The order of current for the PEI-starch-functionalized SWCNTs device can be observed from its *I*−*V* characteristics, as shown in the Supporting Information (Figure S3).

3.3. Gas Sensing Performance of PEI-Starch-Functionalized SWCNTs. To demonstrate real-time tracking of target gases, an ideal gas sensor should respond as the analyte gas flows near the sensing material and then return to its

https://doi.org/10.1021/acsomega.2c06243
ACS Omega 2023, 8, 893−906

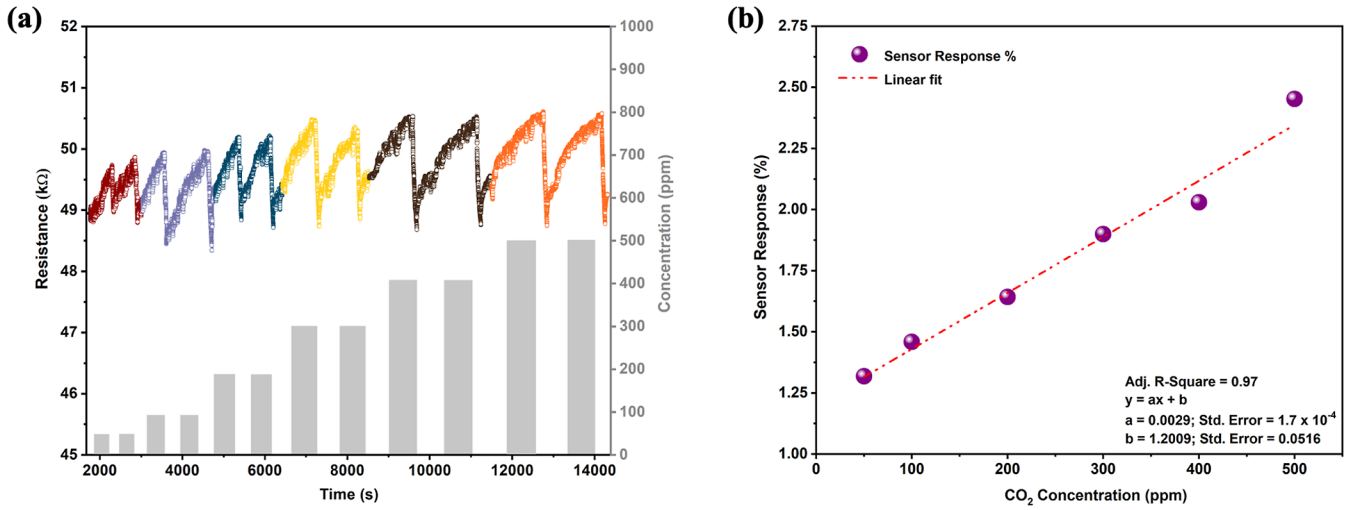

Figure 5. (a) Dynamic sensing responses for the PEI-starch-functionalized SWCNT sensor for a range of CO_2 concentrations (50−500 ppm) at T = 25 °C for V_{bias} = 12 V; (b) Variation of sensor response (%) with CO_2 concentration and its linear fitted curve.

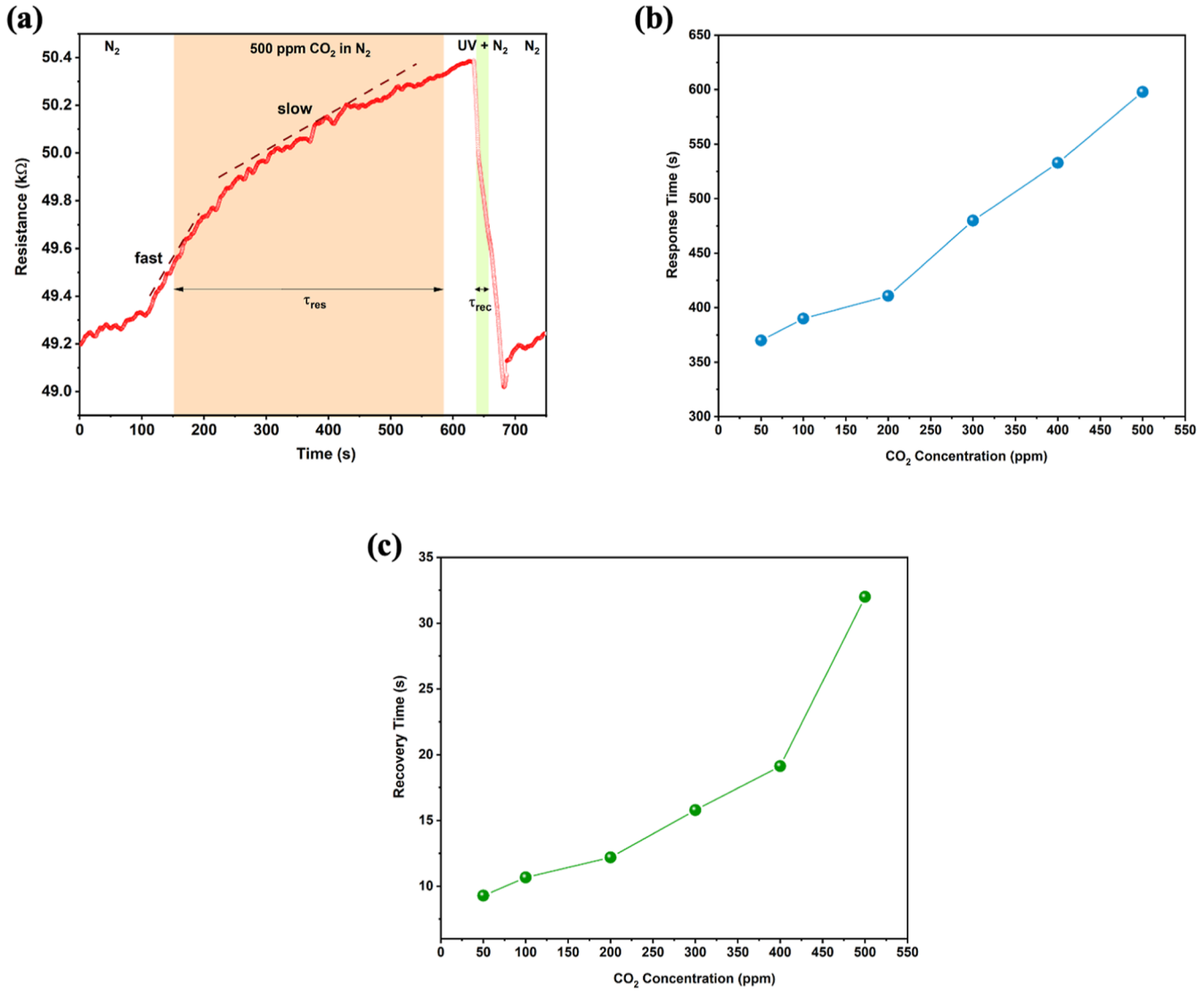

Figure 6. (a) Real-time sensor response and recovery for 500 ppm CO_2 in the background of N_2 flow under ambient room conditions; (b) and (c) Response and recovery times of the sensor device as a function of CO_2 gas concentration, respectively.

https://doi.org/10.1021/acsomega.2c06243
ACS Omega 2023, 8, 893−906

baseline while the gas is evacuated. Prior to investigating the gas sensors' response, both as-grown pristine SWCNTs and PEI-starch functionalized SWCNTbased sensor devices were annealed at 100 °C for 1 h in an inert atmosphere of N_2 gas in order to eliminate fluctuations and noise in resistance transient readings under actual test conditions. Drage et al.[64] have studied about the thermal stability of PEI in a N_2 atmosphere, and it was observed that the thermal degradation of PEI occurs above 135 °C. It was observed that the as-grown pristine SWCNTs sensor device exhibits no change in its resistance on exposure to CO_2 gas at room temperature (See Figure S4).Therefore, it was found that pure SWCNTs-based sensors did not respond to weak Lewis acids or bases, such as CO_2, CH_4, etc., because they had less affinity for these analytes.[41]

3.3.1. Dynamic Sensor Response and Gas Concentration Study. The dynamic responses of the PEI-starch-functionalized SWCNT-based sensor device toward CO_2 exposure were tested at V_{bias} = 12 V for concentrations varying from 50−500 ppm under ambient conditions, as shown in Figure 5a. Prior to the CO_2 filling cycle, the sensing chamber was purged with N_2 gas for half an hour to minimize device contamination. After the device was stabilized, R_0 was considered as the baseline resistance. It was observed that the sensor resistance increases after CO_2 gas adsorption onto the PEI-starch wrapped SWCNTs, and this trend may be explained as follows: SWNTs are p-type semiconducting under ambient conditions due to oxygen molecules adsorbed onto their surfaces,[65,66] but as a result of PEI-starch polymer functionalization, SWCNTs exhibit n-type semiconducting characteristics[67,68] and can effectively capture CO_2 from the gas mixture.[69] CO_2, as a Lewis acid, has a significant tendency to accept additional pairs of electrons from primary and secondary amines of PEI, which is a strong Lewis base[41,70,71] and as a result, the resistance of n-type SWCNT-based sensor increases on CO_2 exposure. *Star* et al.[41] presented in their work the transfer curves of PEI-starch-functionalized SWCNTs and observed no significant variation in threshold voltages before and after exposure to CO_2 gas, which suggests that the rise in sensor resistivity should have occurred due to geometrical distortions in the polymer layer because of the reaction between PEI and CO_2 instead of the charge transfer between PEI and SWCNTs.

Besides, the PEI-starch-functionalized SWCNTs have a strong affinity for capturing CO_2 gas molecules.[69] Therefore, an additional energy source is required to recover the sensor device for successive cycles of gas adsorption either in the form of UV light, heat, or pressure. In this study, we recovered the sensor to its baseline resistance in the presence of UV illumination and N_2 gas flow. As can be observed from Figure 5a, the sensor responses remained fairly constant after every UV recovery process, and the sensor exhibited good reliability.

The effect of CO_2 concentration on gas sensor response (%) was evaluated comprehensively, as shown in Figure 5b. The linear increase in the sensor response with an increase in analyte gas concentration is demonstrated, which may be attributed to the increasing number of adsorption sites available for incoming CO_2 molecules. The gas sensor response as a function of CO_2 concentration can be fitted by a linear function, according to the equation: $S = ax + b$, with adj. R square value close to 1. The slope a of the fitted curve denotes the so-called sensitivity of the sensor and is measured to be 2.9 × 10^{-3} ppm^{-1}, which is competitive across this range of concentration for room-temperature CO_2 sensors.[42] It is, therefore, significant to note that this sensor is capable of operating accurately in a wide range of concentrations.

3.3.2. Sensor Responsiveness Study. The real-time response of the sensor was evaluated by exposing the sensor device to 500 ppm CO_2 until a stable response was achieved, and then the sensor was recovered to its original baseline in the presence of UV and N_2 gas, thus exhibiting reversible gas sensing, as shown in Figure 6a. The response of the sensor can be explained by "fast" and "slow" phases, depending upon the factors of adsorption. The "fast" response is indicative of the reaction kinetics of amine groups of PEI competing in capturing CO_2 molecules. The "slow" response is exhibited due to the diffusion of gas molecules over the available sites for adsorption.[72] The response and recovery times of a sensor are essential parameters for practical applications. The response time (τ_{res}) is the time required for a sensor to attain 90% of the maximum resistance value after exposure to an analyte gas, and the recovery time (τ_{rec}) is the time to arrive at 10% of the final resistance value after the removal of the analyte gas.

The response and recovery times for gas concentrations in a range of 50−500 ppm were calculated from the transient response of the sensor and are plotted in Figure 6b and c. It is noticeable that the response times are nearly in the same range for low concentrations of 50−200 ppm and then increase linearly until they reach a concentration of 500 ppm. This behavior may be explained by the response time (τ_{res}) equation of a reversible gas sensor, which is described as follows

$$\tau_{res} = \frac{1}{k}\left\{\frac{K}{1 + P_g K}\right\} \tag{3}$$

where k is the forward rate constant, K is the reverse rate constant, and P_g is the partial pressure of the analyte gas. The partial pressure of the gas has a direct relationship with the concentration of the gas. For low analyte gas concentrations, eq 3 can be rewritten as[73]

$$\tau_{res}(\lim P_g \to 0) = (\lim P_g \to 0)^{1/k\{\frac{K}{1+P_g K}\}} = \frac{K}{k}(a \text{ constant}) \tag{4}$$

Thus, it can be observed that the deviation of the response time of the sensor at low gas concentrations (50−200 ppm in our study) is minimal and can be regarded as constant with some variation. The linear increase in response time beyond 200 ppm can be suggestive of the slow diffusion of gas molecules onto the limited available binding sites after a certain concentration. The fast recovery of the sensor to its original baseline is carried out in the presence of UV and N_2 gas. This is to ensure that SWCNTs are protected from damage due to UV illumination.[74] The fast recovery characteristics are attributed to the photodesorption caused by UV irradiation, which restored the sensor's initial resistance by inducing molecular desorption. The photon of UV light has enough energy ($h\nu$) to produce electron−hole pairs; $h\nu_{UV} \rightarrow e^- + h^+$. These hot carriers (electrons or holes) may attach to adsorbed molecules and induce rapid desorption.[75,76] The recovery time of the sensor increases slightly at 9−12 s (for 50−200 ppm) and then rises to 32 s for 500 ppm CO_2. It was established that with increasing analyte gas concentration, the ability of the sensing materials to desorb a greater number of gas molecules diminishes, thus leading to increased recovery time. The sensor recovery was also examined in the absence of

https://doi.org/10.1021/acsomega.2c06243
ACS Omega 2023, 8, 893−906

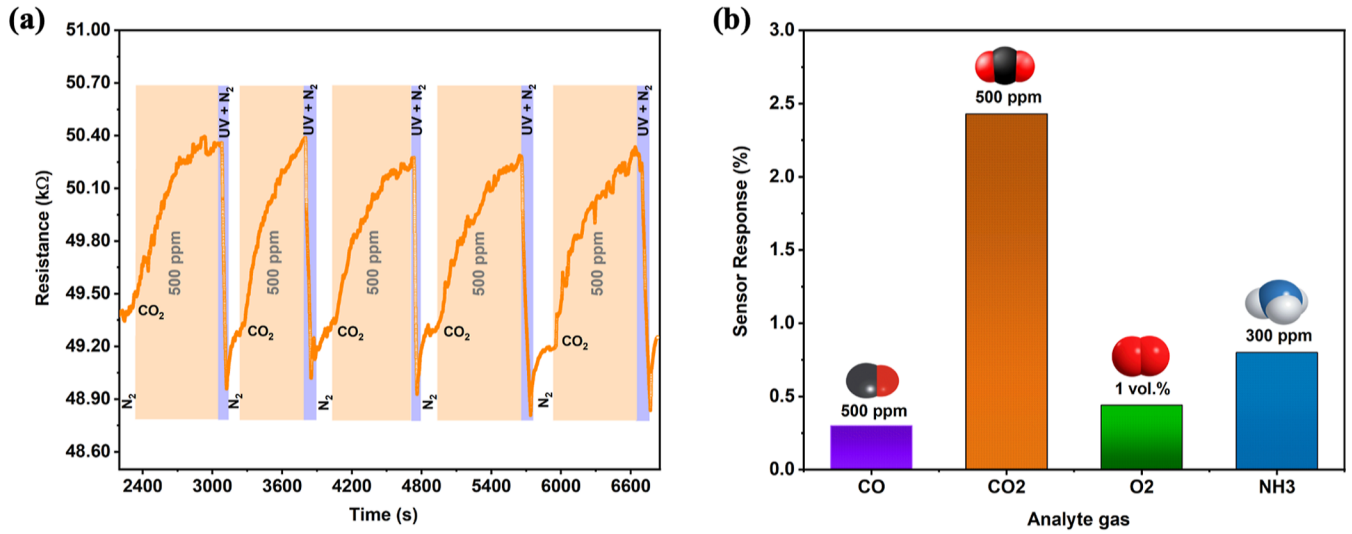

Figure 7. (a) Repeatability of the PEI-starch-functionalized sensor to successive cycles of 500 ppm CO_2 exposure under ambient conditions; (b) Cross-sensitivity histogram of the sensor to different analyte gases at room temperature.

UV irradiation, and it was observed that the sensor exhibited slow and incomplete recovery without UV light (Figure S5). The lower limit of CO_2 gas in air is in a range of 380−400 ppm, and we analyzed the response of the sensor to CO_2 analyte even at 50 ppm. Therefore, it is not necessary to estimate the limit of detection (LOD) of CO_2.

3.3.3. Sensor Repeatability and Cross-Sensitivity Study. The repeatability test of the PEI-starch-functionalized SWCNT sensor was carried out toward 500 ppm CO_2 analyte under ambient conditions for five successive cycles, as shown in Figure 7a. It demonstrates that the sensor can completely recover to its original baseline for a number of repeated cycles, thus exhibiting a stable and reliable response at room temperature. The stability of a sensor was found to be high even after numerous repeated experiments with a high density of CNTs stacked together because of a strong van der Waals interaction. Instead, the low density of individual CNTs achieved in spray-printed CNT sensors led to weaker interactions between CNTs, which eventually led to structural degradation in the CNTs after repeated exposure to test gas.[77] These sensor findings show the developed gas sensor's promise for low-power and low-cost applications.

It is critical to investigate the effect of interfering gases (or distractions) on the response of the sensor. An important sensor parameter determines this property, known as the selectivity or cross-sensitivity of the sensor. In selectivity measurements, the PEI-starch-based SWCNTs sensor was tested against 500 ppm CO, 1 vol.% O_2, and 300 ppm NH_3 under ambient conditions. As seen in Figures S6, S7, and S8, small sensor responses are obtained for these analyte gases. Figure 7b shows a bar graph for the sensor responses when exposed to different analyte gases. The result indicates that the developed sensor is more selective towards carbon dioxide in comparison to other interfering gases. This can be explained by the reaction of CO_2 gas molecules with the amine groups of PEI to attain the acid−base equilibrium condition, resulting primarily in the generation of carbamates and then bicarbonates, or by the direct generation of bicarbonates in the presence of water molecules (due to hygroscopic starch) in the sensing chamber.[68]

3.3.4. Sensing Mechanism: Role of the Hydrophilic Nature of Starch in Improving CO_2 Detection. The sensing mechanism between CO_2 analyte molecules and amine-functionalized CNTs resolves around two probable pathways. One of them is the charge transfer process between CO_2 molecules and the amino groups-functionalized CNTs. *Rahimabady* et al.[78] demonstrated that the exchange of electrons may initially occur between CO_2 molecules and P-MWCNT, and then between the P-MWCNT and the amino groups in diphenylethylenediamine. The second possible pathway depends on the acid−base equilibrium concept.[5,78] According to this theory, when an amide-functionalized material (hard base in nature due to amino groups) interacts with CO_2 gas (hard acid in nature) in the presence of water molecules, the generation of bicarbonate ions protonates the amine groups of the functionalized CNTs and changes the sensor resistance. *Star* et al.[41] strongly proposed the second sensing mechanism in their work due to the negligible change in the transconductance of the PEI-starch-functionalized NTFET device before and after CO_2 adsorption. Therefore, we present a detailed mechanism based on acid−base equilibrium theory and the effect of hydrophilic starch in enhancing CO_2 detection.

To understand the role of hydrophilic starch in sensing, a schematic of the proposed CO_2 sensing mechanism is illustrated in Figure 8 in the absence of starch (a) and in the presence of starch (b). PEI is a highly branched polymer consisting of 25% primary, 50% secondary, and 25% tertiary $-NH_2$ groups alongside the polymeric backbone that induces an n-type characterization of the SWCNTs due to the n-doping effect of PEI on the p-type semiconducting SWCNTs. The electron-donating capacity of amine groups in the polymer as well as the fact that PEI exhibits one of the highest densities of amine groups among the polymers explain the exceptionally efficient n-doping of PEI.[39,42,75] CO_2 is typically an unreactive gaseous species, but it can react with amine moieties at room temperature to form carbamates. This can be explained by the HSAB (Hard Soft Acid Bases) concept, which states that hard base compounds (or different groups of these compounds) tend to bind hard acid compounds, and soft bases tend to attach to soft bases.[70] Since CO_2 is categorized as a hard acid,

https://doi.org/10.1021/acsomega.2c06243
ACS Omega 2023, 8, 893−906

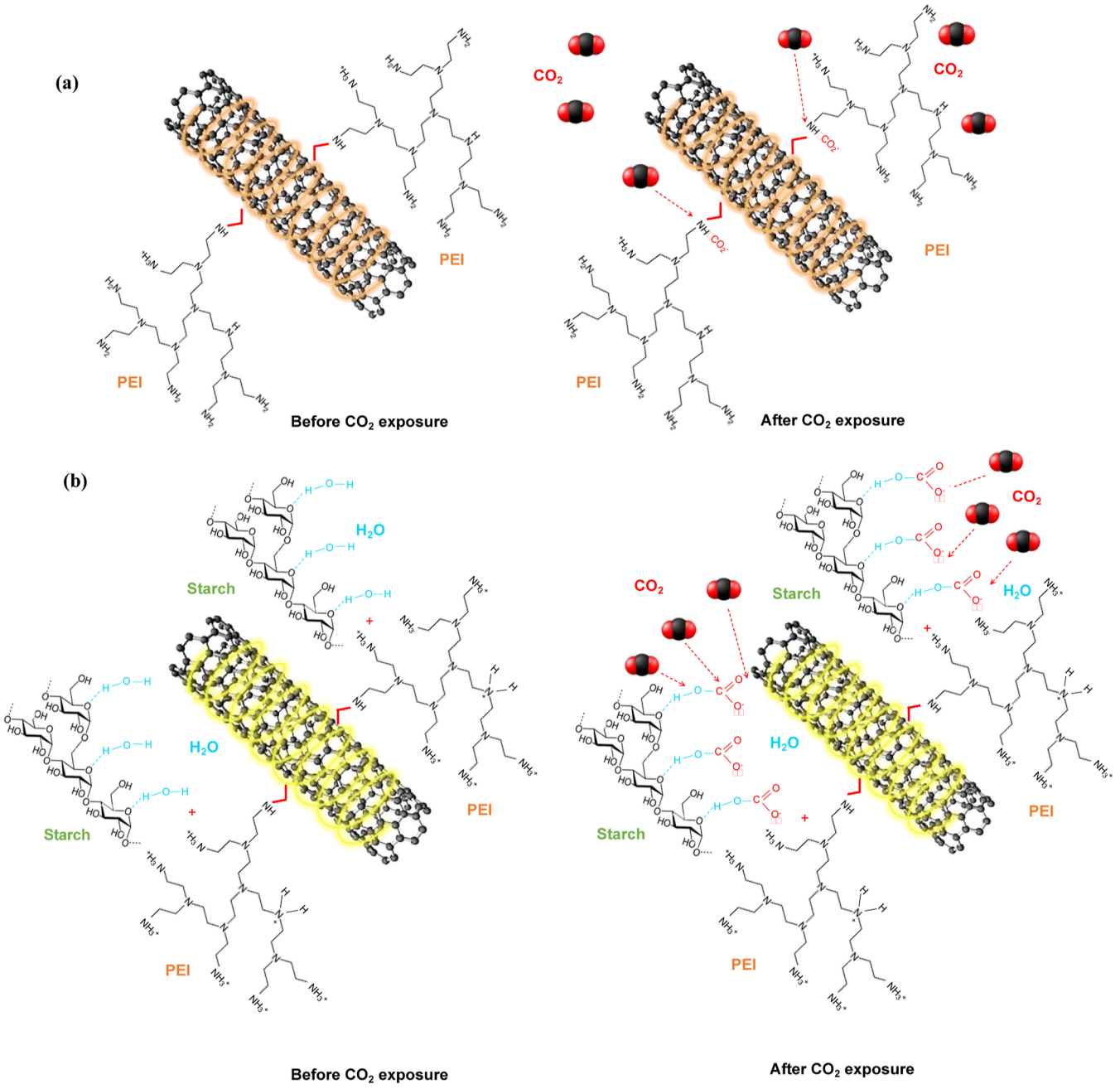

Figure 8. Schematic representation of the proposed CO_2 sensing mechanism under dry conditions (a); and in the presence of hygroscopic starch (b).

it can effectively interact with amine groups in PEI, which are classified as hard bases. On exposure of the PEI-functionalized SWCNTs to analyte CO_2, the primary and secondary amine groups of PEI interact with CO_2 molecules to achieve the acid−base equilibrium condition, leading to the formation of carbamates in the absence of water content. More precisely, a nucleophilic attack by primary and secondary amine groups of PEI on a free CO_2 molecule forms a zwitterion, which reorders itself via intramolecular proton transfer to form carbamic acid. This carbamic acid may again be converted to a carbamate due to the presence of another free amine group (which acts as a Bronsted base) via intermolecular proton transfer. Theoretically, it is observed from eqs 5 and 6 that two mol of amine groups are effective in removing only one mol of CO_2, therefore limiting the adsorption capacity. The reaction pathways between primary/secondary amines and CO_2 are given below

$$CO_2 + 2RNH_2 \leftrightarrow RNH_3^+ + RNHCOO^- \quad (5)$$

$$CO_2 + 2R_2NH \leftrightarrow R_2NH_2^+ + R_2NCOO^- \quad (6)$$

Tertiary amines also do not react with CO_2 directly but rather in the presence of water.Therefore, under dry conditions, further reaction does not occur, and this limits the sensitivity of the PEI-functionalized SWCNTs. Thus, a combination of co-polymers PEI and starch is utilized for the functionalization of SWCNTs. Starch, a mixture of linear chain polymer amylose and branched chain polymer amylopectin,[79] interacts actively with CO_2 and affects its reaction with the amino groups of PEI. Due to the hydrophilic nature of starch,

https://doi.org/10.1021/acsomega.2c06243
ACS Omega 2023, 8, 893−906

Table 2. Comparison of the Gas Sensing Properties of CNT-Based CO_2 Gas Sensors

sensing material	mechanism	temp. (C)	operating environment	CO_2 sensitivity (% ppm^{-1})	response time	recovery time	references
PEI-PEDOT composite film	resistive	RT	RH ~95%, 1000 ppm CO_2 in N_2	2.46×10^{-3}	NA	10 min	[4
CVD-grown graphene	resistive/capacitive	RT	CO_2 and dry gases O_2, N_2, Ar, air	9.1×10^{-6}	3 s	NA	[28
PEI-PANI nanothin film	resistive	RT	RH ~50%, 5000 ppm CO_2 in air	7.14×10^{-3}	7.34 ± 5.21 min	10.01 ± 4.86 min	[5
PEI/NrGO/ZNR porous structure	resistive	RT	RH ~13%, 5 vol % CO_2 in air	2.7×10^{-4}	1−2 min	30 min	[43
nanostructured ZnO thin film	resistive	300	1000 ppm CO_2 in N2	3×10^{-4}	10−20 s	20−40 s	[81
PEI-PEG co-polymer-functionalized graphene	resistive	RT	RH ~60%, 5000 ppm CO_2 in air	$\sim 6.5 \times 10^{-3}$	~80 s	9 min	[82
PEI-PEG/MWCNTs bilayer structure	resistive	RT	RH ~13%, 5 vol % CO2 in air	3.17×10^{-5}	15−30 min	10−20 min	[83
PEI-PEG/CNTs composite film	resistive	RT	RH~50%, 1 vol % CO_2 in N2 flow	2×10^{-4}	~20 min	21−25 s	[42
poly-ionicliquid-$La_2O_2CO_2$ composite film	resistive	RT	RH ~50%, 2400 ppm CO_2 in air	~0.004	~35 min	~40 min	[84
PEI-starch-functionalized CNTs	resistive	RT	10 vol % CO_2 in air	1.01×10^{-4}	~15 s	~15 s	[41
PEI-starch/SWCNTs	resistive	RT	RH ~53%, 500 ppm CO_2 in N_2	$\sim 2.91 \times 10^{-3}$	~9 min	~32 s	this work

more water molecules are attracted to the functionalized SWCNT surface. When the above chemical reactions occur in the presence of hydrophilic starch, the availability of abundant water molecules can further convert carbamates into stable bicarbonate ions, as described in eqs 7 and 8

$$RNHCOO^- + H_2O \leftrightarrow RNH_2 + HCO_3^- \quad (7)$$

$$R_2NCOO^- + H_2O \leftrightarrow R_2NH + HCO_3^- \quad (8)$$

Also, all the three amine groups (primary, secondary, and tertiary) can directly interact with CO_2 and H_2O molecules to form stable bicarbonate ions, as shown in eqs 9−11

$$CO_2 + RNH_2 + H_2O \leftrightarrow RNH_3^+ + HCO_3^- \quad (9)$$

$$CO_2 + R_2NH + H_2O \leftrightarrow R_2NH_2^+ + HCO_3^- \quad (10)$$

$$CO_2 + R_3N + H_2O \leftrightarrow R_3NH^+ + HCO_3^- \quad (11)$$

Thus, water vapor plays a major role in how the co-polymer layer can interact with CO_2, as it acts as a free base, resulting in the formation of bicarbonate ions. Theoretically, it can be observed again from eqs 9−11 that only one mol of amine is effective in removing two mol of CO_2, therefore improving the adsorption capacity. These reversible chemical reactions reduce the total pH of the PEI-starch layer, which depletes the total electron-donating effect of PEI[80] and decreases the charge transfer to the induced n-type semiconducting SWCNTs, thereby resulting in an increase in device resistance, which leads to a sensor response.

To assess the gas sensing performance of this work, we compared our sensing results with those of other CO_2 sensors based on different competent materials. As outlined in Table 2, it is evident that the proposed sensor is a promising candidate for CO_2 detection at room temperature, particularly due to its better sensitivity in comparison to other reported materials.

4. CONCLUSIONS

A PEI-starch-functionalized SWCNT-based sensor was fabricated for chemiresistive CO_2 sensing under ambient room conditions. SWCNTs were grown on the SiO_2/Si substrate by a conventional thermal-chemical vapor deposition technique. The Ti/Au electrode pads were patterned by using conventional photolithography and lift-off processes. The synergic blending of PEI and starch provided an enhanced recognition layer for the reversible adsorption of CO_2. SEM, Raman, and FTIR spectroscopy confirmed the wrapping of SWCNTs and the presence of different functional groups associated with PEI-starch functionalization. The developed gas sensor was tested in the presence of different CO_2 concentrations ranging from 50−500 ppm at room temperature and exhibited an optimal response of 2.43% at 500 ppm of CO_2 gas. The sensing mechanism was based on the reversible acid−base equilibrium reactions between amine groups of PEI and CO_2, leading to the formation of carbamates and bicarbonates. These chemical reactions reduced the overall pH of the polymer layer, decreased electron transfer to n-type SWCNTs, and thereby reduced the device conductance. The response/recovery times varied from 370 s/9 s (at 50 ppm) to 598 s/32 s (at 500 ppm). Complete recovery and shorter recovery times were achieved by using UV illumination in the presence of N_2 gas. The device exhibited stable and reliable responses on repeatable cycles of 500 ppm CO_2 gas at room temperature. Moreover, the device demonstrated excellent cross-sensitivity toward CO_2 in comparison with other interfering gases such as CO, O_2, and NH_3. Therefore, due to their small size, low energy consumption, good sensitivity, and highly stable responses, these sensors are viable alternatives for monitoring the environmental limit of CO_2 under ambient conditions.

■ ASSOCIATED CONTENT

Supporting Information

The Supporting Information is available free of charge at https://pubs.acs.org/doi/10.1021/acsomega.2c06243.

SEM micrographs of as-grown and PEI-starch-functionalized SWCNTs comparing the average diameter of SWCNT bundles, real-time monitoring of resistance versus time for as-grown SWCNTs at T = 100 °C; I−V curve for PEI-starch-functionalized SWCNTs; sensor response of pristine as-grown SWCNTs to 500 ppm CO_2; transient response curve of the PEI-starch

https://doi.org/10.1021/acsomega.2c06243
ACS Omega 2023, 8, 893−906

SWCNT sensor upon 500 ppm CO_2 exposure without UV recovery; and response curves of PEI-starch SWCNT sensor to various gases at room temperature (PDF)

AUTHOR INFORMATION

Corresponding Author

Prabhash Mishra − *Centre for Nanoscience and Nanotechnology, Jamia Millia Islamia (Central University), New Delhi 110025, India; Center for Photonics and 2D Materials, Moscow Institute of Physics and Technology (MIPT), Dolgoprudny 141701, Russia;* orcid.org/0000-0001-9586-6939; Phone: 011-2698-1717 ext. 3229; Email: pmishra@jmi.ac.in

Authors

Samrah Manzoor − *Centre for Nanoscience and Nanotechnology, Jamia Millia Islamia (Central University), New Delhi 110025, India*

Mohammad Talib − *Centre for Nanoscience and Nanotechnology, Jamia Millia Islamia (Central University), New Delhi 110025, India*

Aleksey V. Arsenin − *Center for Photonics and 2D Materials, Moscow Institute of Physics and Technology (MIPT), Dolgoprudny 141701, Russia*

Valentyn S. Volkov − *Center for Photonics and 2D Materials, Moscow Institute of Physics and Technology (MIPT), Dolgoprudny 141701, Russia*

Complete contact information is available at: https://pubs.acs.org/10.1021/acsomega.2c06243

Notes

The authors declare no competing financial interest.

ACKNOWLEDGMENTS

Samrah Manzoor greatly appreciates the financial support from the Department of Science and Technology (DST) India project no. DST/INSPIRE Fellowship/2017/IF170823.Aleksey V. Arsenin, and Prabhash Mishra gratefully acknowledge the financial support from the Ministry of Science and Higher Education of the Russian Federation (no. 0714-2020-0002).Valentyn S. Volkov acknowledges the Russian Science Foundation (no. 22-19-00738) for the support of Raman measurements.

REFERENCES

(1) Prud'homme, A.; Nabki, F. Comparison between Linear and Branched Polyethylenimine and Reduced Graphene Oxide Coatings as a Capture Layer for Micro Resonant CO_2 Gas Concentration Sensors. *Sensors* **2020**, *20*, 1824.

(2) Zito, C. A.; Perfecto, T. M.; Dippel, A. C.; Volanti, D. P.; Koziej, D. Low-Temperature Carbon Dioxide Gas Sensor Based on Yolk−Shell Ceria Nanospheres. *ACS Appl. Mater. Interfaces* **2020**, *12*, 17745−17751.

(3) Turner, R. M.; De Pietro, M.; Ding, B.Overlap of Asthma and Chronic Obstructive Pulmonary Disease in Patients in the United States: Analysis of Prevalence, Features, and Subtypes. *JMIR Public Health & Surveillance***2018**, *4*−60. DOI: 10.2196/publichealth.9930

(4) Chiang, C. J.; Tsai, K. T.; Lee, Y. H.; Lin, H. W.; Yang, Y. L.; Shih, C. C.; Lin, C. Y.; Jeng, H. A.; Weng, Y. H.; Cheng, Y. Y.; Ho, K. C.; Dai, C. A. In Situ Fabrication of Conducting Polymer Composite Film as a Chemical Resistive CO_2 Gas Sensor. *Microelectron. Eng.* **2013**, *111*, 409−415.

(5) Srinives, S.; Sarkar, T.; Hernandez, R.; Mulchandani, A. A Miniature Chemiresistor Sensor for Carbon Dioxide. *Anal. Chim. Acta* **2015**, *874*, 54−58.

(6) Sun, L. B.; Kang, Y. H.; Shi, Y. Q.; Jiang, Y.; Liu, X. Q. Highly Selective Capture of the Greenhouse Gas CO_2 in Polymers. *ACS Sustain. Chem. Eng.* **2015**, *3*, 3077−3085.

(7) *World Meteorological Organization Press Release*, Publ. 25 October 2021, Press Release Number: 2510202.

(8) Shinde, P. V.; Shinde, N. M.; Shaikh, S. F.; Lee, D.; Yun, J. M.; Woo, L. J.; Al-Enizi, A. M.; Mane, R. S.; Kim, K. H. Room-temperature synthesis, and CO_2-gas sensitivity of bismuth oxide nanosensors. *RSC Adv.* **2020**, *10*, 17217.

(9) Liu, K.; Zheng, Z.; Xu, J.; Zhang, C. Enhanced visible light-excited $ZnSnO_3$ for room temperature ppm-level CO_2 detection. *J. Alloys Compd.* **2022**, *907*, 164440.

(10) Yadav, A. A.; Lokhande, A. C.; Kim, J. H.; Lokhande, C. D. Enhanced sensitivity and selectivity of CO_2 gas sensor based on modified La_2O_3 nanorods. *J. Alloys Compd.* **2017**, *723*, 880−886.

(11) Thomas, T.; Ramos Ramón, J. A. R.; Agarwal, V.; Méndez, A. A.; Martinez, J. A. A.; Kumar, Y.; Sanal, K. C. Highly stable, fast responsive Mo_2CT_x MXene sensors for room temperature carbon dioxide detection. *Microporous Mesoporous Mater.* **2022**, *336*, 111872.

(12) Berezkin, V. G. Adsorption Phenomena in Gas-Liquid Chromatography. *J. Chromatogr. A* **1972**, *65*, 227−240.

(13) Beauchamp, J.; Kirsch, F.; Buettner, A. Real-Time Breath Gas Analysis for Pharmacokinetics: Monitoring Exhaled Breath by On-Line Proton-Transfer-Reaction Mass Spectrometry after Ingestion of Eucalyptol-Containing Capsules. *J. Breath Res.* **2010**, *4*, 026006.

(14) Frodl, R.; Tille, T. An automotive bi-source spectroscopic carbon dioxide sensor with pressure compensation. *Sens. Actuator B: Chem.* **2007**, *127*, 82−88.

(15) von Bultzingslöwen, C. V.; McEvoy, A. K.; McDonagh, C.; MacCraith, B. D.; Klimant, I.; Krause, C.; Wolfbeis, O. S. Sol−gel based optical carbon dioxide sensor employing dual luminophore referencing for application in food packaging technology. *Analyst* **2002**, *127*, 1478−83.

(16) Nopwinyuwong, A.; Trevanich, S.; Suppakul, P. Development of a novel colorimetric indicator label for monitoring freshness of intermediate-moisture dessert spoilage. *Talanta* **2010**, *81*, 1126−1132.

(17) Pasierb, P.; Komornicki, S.; Koziński, S.; Gajerski, R.; Rękas, M. Long-term stability of potentiometric CO_2 sensors based on Nasicon as a solid electrolyte. *Sens. Actuators B Chem.* **2004**, *101*, 47−56.

(18) Zhu, Q.; Qiu, F.; Quan, Y.; Sun, Y.; Liu, S.; Zou, Z. Solid-electrolyte NASICON thick film CO2 sensor prepared on small-volume ceramic tube substrate. *Mater. Chem. Phys.* **2005**, *91*, 338−342.

(19) Morio, M.; Hyodo, T.; Shimizu, Y.; Egashira, M. Effect of macrostructural control of an auxiliary layer on the CO_2 sensing properties of NASICON-based gas sensors. *Sens. Actuators B Chem.* **2009**, *139*, 563−569.

(20) Xu, S.; Li, C.; Li, H.; Li, M.; Qu, C.; Yang, B. Carbon dioxide sensors based on a surface acoustic wave device with a graphene-nickel-L-alanine multilayer film. *J. Mater. Chem. C Mater. Opt. Electron. Devices* **2015**, *3*, 3882−3890.

(21) Tanvir, N. B.; Yurchenko, O.; Urban, G. Optimization study for work function-based CO_2 sensing using CuO-nanoparticles in respect to humidity and temperature. *Procedia Eng* **2015**, *120*, 667−670.

(22) Laubender, E.; Tanvir, N. B.; Yurchenko, O.; Urban, G. Nanocrystalline CeO_2 as room temperature sensing material for CO_2 in low power work function sensors. *Procedia Eng* **2015**, *120*, 1058−1062.

(23) Boudaden, J.; Klumpp, A.; Endres, H. E.; Eisele, I. Towards Low Cost and Low Temperature Capacitive CO_2 Sensors Based on Amine Functionalized Silica Nanoparticles. *Nanomaterials* **2019**, *9*, 1097.

(24) Miller, D. R.; Akbar, S. A.; Morris, P. A. Nanoscale metal oxide-based heterojunctions for gas sensing: a review. *Sens. Actuators B Chem.* **2014**, *204*, 250−272.

(25) Xiong, Y.; Xue, Q.; Ling, C.; Lu, W.; Ding, D.; Zhu, L.; Li, X. Effective CO_2 detection based on LaOCl-doped SnO_2 nanofibers: Insight into the role of oxygen in carrier gas. *Sensors and Actuators B* **2017**, *241*, 725−734.
(26) Kanaparthi, S.; Singh, S. G. Chemiresistive Sensor Based on Zinc Oxide Nanoflakes for CO_2 Detection. *ACS Appl. Nano Mater.* **2019**, *2*, 700−706.
(27) Jeong, Y. J.; Balamurugan, C.; Lee, D. W. Enhanced CO_2 Gas-Sensing Performance of ZnO Nanopowder by La Loaded during Simple Hydrothermal Method. *Sens. Actuators B: Chem.* **2016**, *229*, 288−296.
(28) Smith, A. D.; Elgammal, K.; Fan, X.; Lemme, M. C.; Delin, A.; Råsander, M.; Bergqvist, L.; Schröder, S.; Fischer, A. C.; Niklaus, F.; Östling, M. Graphene-based CO_2 sensing and its cross- sensitivity with humidity. *RSC Adv.* **2017**, *7*, 22329.
(29) Wang, Y.; Zhang, K.; Zou, J.; Wang, X.; Sun, L.; Wang, T.; Zhang, Q. Functionalized horizontally aligned CNT array and random CNT network for CO_2 sensing. *Carbon* **2017**, *117*, 263−270.
(30) Li, W.; Yang, H.; Jiang, X.; Liu, Q. Highly Selective CO_2 Adsorption of ZnO Based N-Doped Reduced Graphene Oxide Porous Nanomaterial. *Appl. Surf. Sci.* **2016**, *360*, 143−147.
(31) Kumar, R.; Goel, N.; Kumar, M. UV-Activated MoS_2 Based Fast and Reversible NO_2 Sensor at Room Temperature. *ACS Sens* **2017**, *2*, 1744−1752.
(32) Ou, J. Z.; Ge, W.; Carey, B.; Daeneke, T.; Rotbart, A.; Shan, W.; Wang, Y.; Fu, Z.; Chrimes, A. F.; Wlodarski, W.; Russo, S. P.; Li, Y. X.; Kalantar-zadeh, K. Physisorption-Based Charge Transfer in Two-Dimensional SnS_2 for Selective and Reversible NO_2 Gas Sensing. *ACS Nano* **2015**, *9*, 10313−10323.
(33) Zhang, Y.; Jiang, Y.; Duan, Z.; Wu, Y.; Zhao, Q.; Liu, B.; Huang, Q.; Yuan, Z.; Li, X.; Tai, H. Edge-enriched MoS_2 nanosheets modified porous nanosheet-assembled hierarchical In_2O_3 microflowers for room temperature detection of NO_2 with ultrahigh sensitivity and selectivity. *J. Hazard. Mater.* **2022**, *434*, 128836.
(34) Zhao, Q.; Zhou, W.; Zhang, M.; Wang, Y.; Duan, Z.; Tan, C.; Liu, B.; Ouyang, F.; Yuan, Z.; Tai, H.; Jiang, Y. Edge-Enriched $Mo_2TiC_2T_x/MoS_2$ Heterostructure with Coupling Interface for Selective NO_2 Monitoring. *Adv. Funct. Mater.* **2022**, *32*, 2203528.
(35) Zainab, G.; Iqbal, N.; Babar, A. A.; Huang, C.; Wang, X.; Yu, J.; Ding, B. Free-standing, spider-web-like polyamide/carbon nanotube composite nanofibrous membrane impregnated with polyethyleneimine for CO_2 capture. *Composites Communications* **2017**, *6*, 41−47.
(36) Fennell, J.; Hamaguchi, H.; Yoon, B.; Swager, T. Chemiresistor Devices for Chemical Warfare Agent Detection Based on Polymer Wrapped Single-Walled Carbon Nanotubes. *Sensors* **2017**, *17*, 982.
(37) Zeininger, L.; He, M.; Hobson, S. T.; Swager, T. M. Resistive and Capacitive γ-Ray Dosimeters Based on Triggered Depolymerization in Carbon Nanotube Composites. *ACS Sens* **2018**, *3*, 976−983.
(38) Fong, D.; Andrews, G. M.; Adronov, A. Functionalization of Polyfluorene-Wrapped Carbon Nanotubes via Copper-Mediated Azide-Alkyne Cycloaddition. *Polym. Chem.* **2018**, *9*, 2873−2879.
(39) Han, M.; Jung, S.; Lee, Y.; Jung, D.; Kong, S. H. PEI-Functionalized Carbon Nanotube Thin Film Sensor for CO_2 Gas Detection at Room Temperature. *Micromachines* **2021**, *12*, 1053.
(40) Bag, S.; Pal, K. Sulfonated poly (ether ether ketone) based carbon dioxide gas sensor: Impact of sulfonation degree on sensing behavior at different humid condition. *Sensors & Actuators: B. Chemical* **2020**, *303*, 127115.
(41) Star, A.; Han, T. R.; Joshi, V.; Gabriel, J. C. P.; Grüner, G. Nanoelectronic carbon dioxide sensors. *Adv. Mater.* **2004**, *16*, 2049−2052.
(42) Siefker, Z. A.; Zhao, X.; Bajaj, N.; Boyina, A.; Braun, J. E.; Chiu, G. T. C.; Boudouris, B. W.; Rhoads, J. F.A Carbon Nanotube-Functional Polymer Composite Film for Low-Power Indoor CO_2 Monitoring. *IEEE Sensors***2022**, *22*−12., No. DOI: 10.1109/jsen.2021.3131428
(43) Tripathy, A. R.; Chang, C.; Gupta, S.; Anbalagan, A. K.; Lee, C. H.; Li, S. S.; Tai, N. H. Polyethylenimine/Nitrogen-Doped Reduced Graphene Oxide/ZnONanorod Layered Composites for Carbon Dioxide Sensing at Room Temperature. *ACS Appl. Nano Mater.* **2022**, *5*, 6543−6554.
(44) Jadhav, P.; Chatti, R.; Biniwale, R.; Labhsetwar, N.; Devotta, S.; Rayalu, S. Monoethanol Amine Modified Zeolite 13X for CO_2 Adsorption at Different Temperatures. *Energy Fuels* **2007**, *21*, 3555−3559.
(45) Garg, R.; Agarwal, A.; Agarwal, M. A review on MXene for energy storage application: effect of interlayer distance. *Mater. Res. Express* **2020**, *7*, 022001.
(46) Radhakrishnan, J. K.; Kumara, M.; Geetika, M. Effect of temperature modulation, on the gas sensing characteristics of ZnO nanostructures, for gases O_2, CO and CO_2. *Sensors International* **2021**, *2*, 100059.
(47) Bandow, S.; Kokai, F.; Takahashi, K.; Yudasaka, M.; Qin, L. C.; Iijima, S. Interlayer spacing anomaly of single-wall carbon nanohorn aggregate. *Chem. Phys. Lett.* **2000**, *321*, 514−519.
(48) Xiaohui, M.; Luo, L.; Zhu, L.; Yu, L.; Sheng, L.; An, K.; Ando, Y.; Zhao, X. Pt-Fe catalyst nanoparticles supported on single-wall carbon nanotubes: Direct synthesis and electrochemical performance for methanol oxidation. *J. Power Sources* **2013**, *241*, 274−280.
(49) Jorio, A.; Saito, R.; Dresselhaus, G.; Dresselhaus, M. S. Determination of nanotubes properties by Raman spectroscopy. *Phil. Trans. R. Soc. Lond. A* **2004**, *362*, 2311−2336.
(50) Jorio, A.; Saito, R. Raman spectroscopy for carbon nanotube applications. *J. Appl. Phys.* **2021**, *129*, 021102.
(51) Kupka, T.; Stachów, M.; Stobiński, L.; Kaminský, J. Calculation of Raman parameters of real-size zigzag (n, 0) single-walled carbon nanotubes using finite-size models. *Phys. Chem. Chem. Phys.* **2016**, *18*, 25058.
(52) Lu, H.; Zhang, A.; Zhang, Y.; Ding, L.; Zheng, Y. The effect of polymer polarity on the microwave absorbing properties of MWNTs. *RSC Adv.* **2015**, *5*, 64925−64931.
(53) Zhao, Q.; Wagner, D. H. Raman spectroscopy of carbon−nanotube−based composites. *Phil. Trans. R. Soc. Lond. A* **2004**, *362*, 2407−2424.
(54) Hussain, S.; Jha, P.; Chouksey, A.; Raman, R.; Islam, S. S.; Islam, T.; Choudhary, P. K.; Choudhary, P. K. Spectroscopic Investigation of Modified Single Wall Carbon Nanotube. *Journal of Modern Physics* **2011**, *02*, 538−543.
(55) Zaaeri, F.; Khoobi, M.; Rouini, M.; Akbari Javar, H. pH-responsive polymer in a core−shell magnetic structure as an efficient carrier for delivery of doxorubicin to tumor cells. *Int. J. Polym. Mater. Polym. Biomater.* **2018**, *67*, 967−977.
(56) Li, K.; Zhang, C.; Du, Z.; Li, H.; Zou, W. Preparation of humidity-responsive antistatic carbon nanotube/PEI nanocomposites. *Synth. Met.* **2012**, *162*, 2010−2015.
(57) Liu, H.; Kuila, T.; Kim, N. H.; Ku, B. C.; Lee, J. H. In Situ Synthesis of the Reduced Graphene Oxide−Polyethyleneimine Composite and Its Gas Barrier Properties. *J. Mater. Chem. A* **2013**, *1*, 3739−3746.
(58) Wang, F.; Liu, P.; Nie, T.; Wei, H.; Cui, Z. Characterization of a Polyamine Microsphere and its Adsorption for Protein. *Int. J. Mol. Sci.* **2013**, *14*, 17−29.
(59) Duan, X.; Duan, Z.; Zhang, Y.; Liu, B.; Li, X.; Zhao, Q.; Yuan, Z.; Jiang, Y.; Tai, H. Enhanced NH_3 sensing performance of polyaniline via a facile morphology modification strategy. *Sensors & Actuators: B. Chemical* **2022**, *369*, 132302.
(60) Sadegh, H.; Shahryari-ghoshekandi, R.; Kazemi, M. Study in synthesis and characterization of carbon nanotubes decorated by magnetic iron oxide nanoparticles. *Int Nano Lett* **2014**, *4*, 129−135.
(61) Jishi, R. A.; Venkataraman, L.; Dresselhaus, M. S.; Dresselhaus, G. Phonon modes in carbon nanotubules. *Chem. Phys. Lett.* **1993**, *209*, 77−82.
(62) Kong, J.; Yenilmez, E.; Tombler, T. W.; Kim, W.; Dai, H. J.; Laughlin, R. B.; Liu, L.; Jayanthi, C. S.; Wu, S. Y. Quantum Interference and Ballistic Transmission in Nanotube Electron Waveguides. *Phys. Rev. Lett.* **2001**, *87*, 106801.

(63) Tizani, L.; Abbas, Y.; Yassin, A. M.; Mohammad, B.; Rezeq, M. Single wall carbon nanotube based optical rectenna. *RSC Adv.* **2021**, *11*, 24116−24124.
(64) Drage, T. C.; Arenillas, A.; Smith, K. M.; Snape, C. E. Thermal stability of polyethylenimine based carbon dioxide adsorbents and its influence on selection of regeneration strategies. *Microporous Mesoporous Mater.* **2008**, *116*, 504−512.
(65) Javey, A.; Shim, M.; Dai, H. Electrical properties and devices of large-diameter single walled carbon nanotubes. *Appl. Phys. Lett.* **2002**, *80*, 1064−1066.
(66) Kang, D.; Park, N.; Ko, J. H.; Bae, E.; Park, W. Oxygen-induced p-type doping of a long individual single-walled carbon nanotube. *Nanotechnology* **2005**, *16*, 1048.
(67) Shim, M.; Javey, A.; Shi Kam, N. W. S.; Dai, H. Polymer functionalization for air- stable n-type carbon nanotube field-effect transistors. *J. Am. Chem. Soc.* **2001**, *123*, 11512−11513.
(68) Qi, P. F.; Vermesh, O.; Grecu, M.; Javey, A.; Wang, O.; Dai, H.; Peng, S.; Cho, K. J. Toward large arrays of multiplex functionalized carbon nanotube sensors for highly sensitive and selective molecular detection. *Nano Lett.* **2003**, *3*, 347−351.
(69) Satyapal, S.; Filburn, T.; Trela, J.; Strange, J. Performance and properties of a solid amine sorbent for carbon dioxide removal in space life support applications. *Energy Fuels* **2001**, *15*, 250−255.
(70) Jensen, W. B.*The Lewis Acid-base Concepts: An Overview*; Wiley: New York, 1980.
(71) Rezk, M. Y.; Sharma, J.; Gartia, M. R. Nanomaterial-Based CO_2 Sensors. *Nanomaterials (Basel)* **2020**, *10*, 2251.
(72) Shadi, S. S.; Guillemette, J.; Guermoune, A.; Siaj, M.; Szkopek, T. Enhancing gas induced charge doping in graphene field effect transistors by non- covalent functionalization with polyethyleneimine. *Appl. Phys. Lett.* **2012**, *100*, 113106.
(73) Mukherjee, K.; Gaur, A. P. S.; Majumder, S. B. Investigations on Irreversible- and Reversible-type Gas Sensing for ZnO and $Mg_{0.5}Zn_{0.5}Fe_2O_4$ Chemi-resistive Sensors. *J. Phys. D: Appl. Phys.* **2012**, *45*, 505306.
(74) Chen, G.; Paronyan, T. M.; Pigos, E. M.; Harutyunyan, A. R. Enhanced gas sensing in pristine carbon nanotubes under continuous ultraviolet light illumination. *Sci. Rep.* **2012**, *2*, 343.
(75) Shim, M.; Javey, A.; Shi Kam, N. W. S.; Dai, H. Polymer Functionalization for Air-Stable n-Type Carbon Nanotube Field-Effect Transistors. *J. Am. Chem. Soc.* **2001**, *123*, 11512−11513.
(76) Jeon, J. Y.; Kang, B. C.; Byun, Y. T.; Ha, T. J. High-performance gas sensors based on single-wall carbon nanotube random networks for the detection of nitric oxide down to the ppb-level. *Nanoscale* **2019**, *11*, 1587.
(77) Han, M.; Kim, J.; Kang, S.; Jung, D. Post-treatment effects on the gas sensing performance of carbon nanotube sheet. *Appl. Surf. Sci.* **2019**, *481*, 597−603.
(78) Rahimabady, M.; Tan, C. Y.; Tan, S. Y.; Chen, S.; Zhang, L.; Chen, Y. F.; Yao, K.; Zang, K.; Humbert, A.; Soccol, D.; Bolt, M. Dielectric nanocomposite of diphenylethylenediamine and P-type multi-walled carbon nanotube for capacitive carbon dioxide sensors. *Sens. Actuators B Chem.* **2017**, *243*, 596−601.
(79) (a) Collins, P.; Ferrier, R.*Polysaccharides: Their Chemistry*; John Wiley & Sons: Chichester, U.K., 1995, p 478. (b) Lehmann, J.*Carbohydrates Structure and Biology*; Georg Thieme Verlag: Stuttgart, Germany, 1998, p 98. (c) Thompson, D. B. On the non-random nature of amylopectin branching. *Carbohydr. Polym.* **2000**, *43*, 223.
(80) Zhang, K.; Zou, J. P.; Zhang, Q. Roles of inter-SWCNT junctions in resistive humidity response. *Nanotechnology* **2015**, *26*, 455501.
(81) Kannan, P. K.; Saraswathi, R.; Rayappan, J. B. B. CO_2 Gas Sensing Properties of DC Reactive Magnetron Sputtered ZnO Thin Film. *Ceram. Int.* **2014**, *40*, 13115−13122.
(82) Son, M.; Pak, Y.; Chee, S. S.; Auxilia, F. M.; Kim, K.; Lee, B. K.; Lee, S.; Kang, S. K.; Lee, C.; Lee, J. S.; et al. Charge Transfer in Graphene/Polymer Interfaces for CO_2 Detection. *Nano Res.* **2018**, *11*, 3529−3536.
(83) Lin, C. C.; Gupta, S.; Chang, C.; Lee, C. Y.; Tai, N. H. Polyethylenimine-Polyethylene Glycol/Multi-Walled Carbon Nanotubes Bilayer Structure for Carbon Dioxide Gas Sensing at Room Temperature. *Mater. Lett.* **2021**, *297*, 129941.
(84) Willa, C.; Yuan, J.; Niederberger, M.; Koziej, D. When Nanoparticles Meet Poly (Ionic Liquid)s: Chemoresistive CO_2 Sensing at Room Temperature. *Adv. Funct. Mater.* **2015**, *25*, 2537−2542.

https://doi.org/10.1021/acsomega.2c06243
ACS Omega 2023, 8, 893−906